Multi-wavelength speciation of high-temperature 1-butene pyrolysis

Nicolas H. Pinkowski[*], Séan J. Cassady, David F. Davidson, Ronald K. Hanson

High Temperature Gasdynamics Laboratory, Department of Mechanical Engineering, Stanford

University, Stanford, CA 94305-3032, USA

Abstract

Species time-history measurements provide important kinetics targets for the development and validation of detailed reaction models. Here, a multi-wavelength, multi-species laser absorption strategy is demonstrated that provides high-bandwidth species time-histories during 1-butene pyrolysis behind reflected shock waves. Measured shock tube absorbance traces at nine wavelengths were used to resolve nine species mole fractions in the pyrolysis of 5% 1-butene in argon at 1300 K, 1.8 atm. In addition to existing sensors for 1-butene, methane, ethylene, 1,3-butadiene, propene, allene, benzene, and cyclopentadiene, a new laser absorption sensor for ethane at 3.3519 µm was developed by measuring cross-sections of ethane and of expected major interferers. Additional measurements to complete a square absorption cross-section matrix were also performed that enabled the simultaneous solution of species mole fractions from absorbance time-histories under appropriate physical system constraints. Measured time-histories of the nine product species were also compared with existing flow-reactor-based kinetic mechanisms. The demonstrated method has further application potential in the speciation of larger, more complex fuels.

Keywords: 1-butene, hydrocarbon pyrolysis, high temperature, time-resolved, laser absorption spectroscopy, cross-sections, ethane diagnostic, shock tubes

1. Introduction

[*] Corresponding Author
Email address: npinkows@stanford.edu

25

In recent years, efforts to improve detailed kinetic models have motivated the development of advancedspeciation techniques inhigh-temperature studies of hydrocarbon fuels[1].In particular, therecently introduced hybrid chemistry modeling approach known as HyChem relies on accurate species time-history measurements during the thermal decomposition of hydrocarbons [2–5]. At the shorttimescales needed to resolve such fast pyrolysis chemistry, shock tube facilitiescan provide a wide range of well-controlled experimental conditions, and laser absorption spectroscopy offers a high-bandwidth measurement technique for resolving the formation and removal of individual species[6,7]. Historically, laser absorption at3.392 µm has been a popular choice for measuring time-histories of fuels in shock tube kinetics research[8–11]. However, the measured absorbance at any single wavelength may result from the composite absorption of a blend of species with overlapping spectral features, a phenomenon that can obfuscate the determination of individual time-histories in real-fuel experiments.To circumvent this challenge, carefullyselected diagnostic wavelengths have been developed to enable targeted measurements of individual species such as methane [12,13], ethylene [14–16], acetylene[17], and iso-butene[18]. In cases where discrete, narrow features are measured, the two-color online/offline technique described in [13]can be used to subtract spectral interference from larger absorbers.

However, for species with broader features, such a technique is not always possible. Instead, multi-wavelength diagnostic techniques have been developed for resolving multiple species simultaneously. For example, Parise et al. [19]present a two-wavelength, two-species diagnostic measuring ethylene and propene, and a three-wavelength version that includes iso-butene[20]. In such multi-wavelength speciation methods, measured species serve as unknowns in the simultaneous solution of a system of equations (wavelengths). In fact, the online/offline technique can be thought of as a special case of multi-wavelength speciation: under the assumption of flat interfering absorbance, the online and offline wavelengths provide two equations for two unknowns (absorbance from the target species, and that of all other interferers). Recently, Pinkowski et al. [21]have extended this technique to any number of species

within a convex optimization framework. They compiled adatabase of cross-sections for eleven species at eleven sensitive wavelengths, many of which have been used for standalone diagnostics in the works cited above. The present study represents the first demonstration of this method with application to the pyrolysis of the smallest alkene with an isomeric structure: 1-butene. However, literature data on 1-butene pyrolysis in a flow reactor [22] predicts the formation of a measurable amount of ethane, for which this speciation effort must account. Consequently, the goals of the present work are (1) to provide species time-histories at representative conditions during the high-temperature pyrolysis of 1-butene, (2) to develop a new wavelength for sensitive measurements of ethane in a shock tube, (3) to supplement the cross-section matrix of [21]with species and wavelengths relevant to 1-butene pyrolysis, and (4) demonstratethe convex speciation method described in[21].

2. Background

2.1. Laser absorption spectroscopy

Laser absorption spectroscopy leveragesthe propensity of matter to absorb lightto enablequantitative measurements of species gas properties.Shown in Eq. 1,the Beer-Lambert equation relates the attenuation ofmonochromatic light at wavelength λ to the number density of a species. Absorbance (α) is defined as the negative natural logarithm of the transmission (I/I_0). The absorbance is related to the product of the number density of the i^{th}species (n_i) and measurement path length(L) through a proportionality factor (σ) known as absorption cross-section. The absorption cross-section is a wavelength-, temperature-, pressure-, and composition-dependent property of a species that describes its interaction with light.

$$\alpha_\lambda = -\ln\left(\frac{I}{I_0}\right) = n_i\sigma_\lambda L \tag{1}$$

75

76   Eq. 1 presents a formulation of the Beer-Lambert relation that assumes the presence of only a single

77   absorbing species at a given wavelength. However, when multiple species are present, the absorption

78   spectrum of each canexhibit appreciable overlap.Therefore, the absorbance$\alpha_\lambda$at

79   wavelengthλbecomesthecomposite absorbancecontributed by all constituents. Isolating and studying one

80   species among a variegated blend presents a challenge for kinetics studies. To supportthe determination

81   of mole fractions from blended absorbance measurements,a variety of simultaneouslyprobedwavelengths

82   can be used to discern between the unique spectral shapes of each individual absorber. In principle, if N

83   absorbing species are present, at least$N$ wavelengthsof light are needed to create a system of linear

84   equations that can be solved for the mole fraction of all species. Eq. 2 presents representation of

85   thevectorized formulation of the Beer-Lambert relation for N species and M wavelengths, with x

86   denoting mole fraction.

87

$$\sigma_{CH4,\lambda_1}x_{CH4} + \sigma_{C2H4,\lambda_1}x_{C2H4} + \cdots \sigma_{N,\lambda_1}x_i = \frac{\alpha_{\lambda_1}}{nL}$$

$$\sigma_{CH4,\lambda_2}x_{CH4} + \sigma_{C2H4,\lambda_2}x_{C2H4} + \cdots \sigma_{N,\lambda_2}x_i = \frac{\alpha_{\lambda_2}}{nL} \tag{2}$$

$$\vdots$$

$$\sigma_{CH4,\lambda_M}x_{CH4} + \sigma_{C2H4,\lambda_M}x_{C2H4} + \cdots \sigma_{N,\lambda_M}x_i = \frac{\alpha_{\lambda_M}}{nL}$$

88

89   A convex speciation framework has been proposed by Pinkowski et al.[21] to enable the

90   simultaneous calculation of mole fractions from a blended set of absorbance measurements. A cross-

91   section matrix $\{K \in \mathbb{R}^{M\times N}\}$ (m^{2}mol^{-1}), mole fraction vector $\{\vec{x} \in \mathbb{R}^N\}$, and normalized absorbance

92   vector $\{\vec{b} \in \mathbb{R}^M \mid \vec{b} = \vec{\alpha}/nL\}$ (m^{2}mol^{-1}) are established and minimized under constraints.Eq. 3 presents

93   the objective function and constraints used in the current study.Eq. 3 is solved for a vector of mole

94 fractions using CVX software from CVX Research Inc. [23,24]. Because temperature, and consequently

95 number density, were not well-known in the present study, the system was solved using the absorption

96 coefficient matrix k (atm^{-1}cm^{-1}) and pressure-normalized vector $\vec{b} = \vec{\alpha}/PL$ (atm^{-1}cm^{-1}) instead of their

97 cross-sectional counterparts (defined in terms of m^2 mol^{-1}). Both methods are equivalent; the latter

98 simply uses more readily measured quantities in its solution.

99

(3)

$$Minimize \; \left\| k\vec{x} - \vec{b} \right\|_2^2$$

Subject to:

1) $\vec{x} \geq 0$

2) The calculated number of hydrogen and
   carbon atoms must not exceed the known
   amount at time-zero

3) $k\vec{x} \leq \vec{b}$

100 Three constraints are used in the solution of $\vec{x}$: (1) that the mole fractions must be positive, (2) that

101 the calculated number of atoms must not exceed the known number of atoms at time-zero, and (3) that

102 the sum of the absorbance contribution from each species must be less than or equal to the measured

103 absorbance at each wavelength. The first and second constraints enforce physically valid mole fractions

104 and the third constraint asserts that no combination of species can absorb more than measured. The third

105 constraint creates a system that is robust to interfering absorbers by imposing only positive or zero

106 unaccounted absorbance of magnitude $(\vec{b} - k\vec{x})$ (atm^{-1}cm^{-1})

107

108 *2.2. Shock tube facilities*

109

110   Two pressure-driven, stainless steel shock tubes of comparable bore (13.97 cm and 14.13 cm) were

111   used in the current study to facilitate measurements of cross-sections and species time-histories. The two

112   shock tubes consist of2.8 meter- and 3.35 meter-longhigh-pressure driver gas regions, respectively, and

113   9.5/8.54 meter-long regions for low-pressure driven gas. Polycarbonate diaphragms between 0.125 mm

114   and 0.25 mm were used to separateeach regionand were designed to burst with a pressure differential

115   between 1 and 3 atm. Each shock tube uses a reflected shock wave to nearlyinstantaneously generate a

116   well-controlled region of high temperature and pressure near the endwall of the driven section. The

117   initial temperature, pressure, and composition of the test gas, along with measurements of the incident

118   shock velocity from five pressure transducerslocated along the length of the driven section, are all used

119   to determine the thermodynamic state of the gas at time-zero, when the reflected shock passes the

120   measurement plane. In the present work, a shock condition calculator developed by Campbell et al.

121   [25]was used to calculate these conditions. The calculator uses the shock jump equations along with

122   assumptions of frozen chemistry anda vibrationallyrelaxedsystemafter the incident and reflected

123   shock.Supporting the validity of both assumptions, good agreement wasobserved between measured and

124   calculated pressures in the present study. Additional support is found in the literature in similar shock

125   tube work[26].

126

127   *2.3. Laser systems*

128

129   Nine lasers, each emitting light at distinct wavelengths in the 3 µm and 10 µm regions, were aligned

130   through one of the two shock tubes to capture absorption time-histories across a range of conditions.

131   Each shock tube had six optical ports offering three lines-of-sight through which one or two lasers were

132   simultaneously aligned. In total, three separate optical configurations were constructed between both

133   shock tubes to enable measurements of all conditions with all lasers. Experimental tests were duplicated

134   with at least one common laser in each successive configuration to ensure consistent absorption

135   measurements throughout the entire experimental domain. Lasers were chosen with output wavelengths

136 strongly sensitive to methane (tunable interband cascade laser (ICL), online/offline: 3.1758 µm/3.17595

137 µm [12]), aromatics (ICL, 3.283 µm [21]),ethane (ICL, 3.3519 µm, new in this work), ethylene (CO_2 gas

138 laser, 10.532 µm [14]), and propene (external cavity quantum cascade laser (EC-QCL), 10.958 µm [19]).

139 Additional wavelengths to further discern individual species were selected by considering the

140 availability of cross-section data, unique cross-sectional features, and laser accessibility: the He-Ne laser

141 output at 3.392 µm[10,11,27,28], CO_2 gas laser wavelength 10.675 µm [15], and 11.325 µm from an

142 EC-QCL[18]. A Bristol 721 spectrum analyzer was used to confirm the wavelengths of all lasers before

143 each experiment.

144 To support the sensitive detection of ethane, a new fixed-wavelength diagnostic at 3.3519 µm was

145 developed in this work. A detailed discussion of the wavelength-selection process and resulting cross-

146 sections can be found in Appendix A.

147
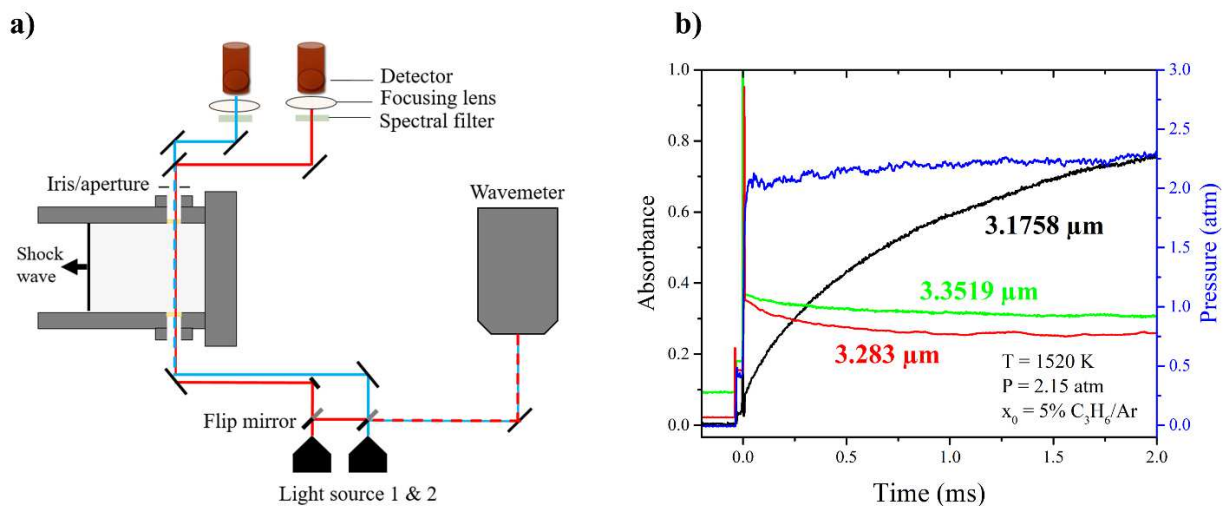
148

149

150 **Fig. 1**. (a) Experimental setup of two lasers aligned through one window of a shock tube. (b) Example

151 absorbance and pressure measurements from a shock tube experiment of 5% propene (C_3H_6) in argon

152 and an initial temperature of 1520 K.

153

154   Fig.1(a) shows a representative two-dimensional schematic of a shock tube facility instrumented

155   with laser diagnostics for kinetics studies. Laser light traverses the test section of the tube through two

156   optical ports and is focused onto individual detectors. Laser measurements near 3 µm generally use

157   sapphire window ports, while systems with laser light near 10 µm use zinc selenide windows. In the

158   present study, all optical setups included narrow-bandpass spectral filters to mitigate detection of thermal

159   emission from the high-temperature gases. Focusing optics were used immediately before either liquid

160   nitrogen-cooled photovoltaic indium antimonide detectors for 3-4 µm light or thermoelectricallycooled

161   photovoltaic mercury cadmium telluride detectors for 10-12 µm light. Example absorption data for the

162   pyrolysis of propene behind a reflected shock wave are shown in Fig. 1(b). Three lasers probing discrete

163   wavelengths in the 3 µm region gather information about species formation and removal. Absorbance at

164   3.1758 µm, shown in black in Fig.1(a), is largely attributed to the formation of methane. The two other

165   wavelengths indicated in Fig. 1(a), of 3.3519 µm (green) and 3.283 µm (red), measure absorption from a

166   variety of different C-H vibrational stretch modes with competing intensities.

167

168   *2.4. 1-butene pyrolysis*

169

170   There is a continuing interestin improvingreaction mechanisms for the pyrolysis and oxidation

171   kinetics of butanols, large alkanes (such as n-heptane and iso-octane), and practical fuels such as Jet A.

172   For each of thesefuels, 1-butene is known to be an important intermediate species and pyrolysis product,

173   but despite 1-butene's importance in such mechanisms,only a limited number of studies of high-

174   temperature 1-butene kineticsexist. In the last decade, flow reactor experiments performed byShoaibi et

175   al. [29], Zhang et al. [30], and Wang et al. [22]have guidedthe development of butene-

176   specificreactionmechanisms.Wang et al. [22] and others[31,32]indicate that fuel fragments from

177   pyrolysis have a strong effect in determining oxidation kinetics.Therefore, characteristics of ignition

178   chemistry can be better understood through an improved understanding of pyrolysis processes.

179   Time-resolved speciation is needed for further refinement of the rate constants that dominate $1\text{-}C_4H_8$

180   reaction pathways. Although flow reactors can provide sensitive speciation measurements,limited

181   temporal resolution has inhibitedtheir application to high-temperature chemistry. Single pulse shock tube

182   speciation studies have also been conducted, relying on post-reaction samples to determine pyrolysis

183   yields [33]; however, these frozen samples provide limited insight into early-time reaction pathways. To

184   the authors' knowledge, no laser absorption spectroscopy speciation studies of 1-butene pyrolysis have

185   been conducted, likely due to the heavilyblended spectra of the hydrocarbon products. The recent

186   establishment of a high-temperature spectroscopic cross-section database and a convex speciation

187   framework have enabled the separation of individual species from blended absorption measurements.

188   Data from the literature[22,29,30,33–36] predict the dominant products of 1-butene pyrolysis to be

189   methane (CH_4), ethylene (C_2H_4), propene (C_3H_6), 1,3-butadiene ($1,3\text{-}C_4H_6$), ethane (C_2H_6), allene

190   (aC_3H_4), benzene (C_6H_6), and cyclopentadiene (C_5H_6). To enable the detection of these predicted major

191   species, a new wavelength was included to leverage strong absorption by ethane in the $3 – 4$ μm region,

192   and cross-sections of all nine species were measured, determined from the literature, or estimated at each

193   wavelength used.

194

195   **3.   Multi-wavelength cross-section matrix**

196

197   Multi-wavelength speciation methods rely on a collection of high-temperature absorption cross-

198   section measurements at each probed wavelength for all species of interest.In the current study, a nine-

199   species, nine-wavelength absorption cross-section matrix was used to account for the cross-sections of

200      $CH_4, C_2H_4, C_2H_6, C_3H_6, aC_3H_4$ (allene), $1\text{-}C_4H_8, C_4H_6$ (1,3-butadiene), C_5H_6 (cyclopentadiene), and C_6H_6

201   (benzene) at 3.1758 μm, 3.17595 μm, 3.283 μm, 3.3519 μm, 3.392 μm, 10.532 μm, 10.675 μm, 10.958

202   μm,and 11.345 μm. Temperature- and occasionally, pressure-dependent cross-section correlations were

203   required for the 81 cells of the matrix. Appendix B presents the collection of absorption cross-

204   sectionsused to speciate 1-butene pyrolysis. The quantified uncertainty of each cross-section

measurement is particularly important in facilitating a thorough uncertainty quantification of the resulting mole fraction time-histories. For one species, allene, many cross-section approximations were required. However, the majority of the allene absorption cross-sections are predicted to be near zero. In instances where allene absorbs appreciably, such as at 10.958 µm and 11.345 µm, the absorption cross-sections were either known from [37] or approximated from lower-temperature FTIR data. Ultimately, perturbing these approximated cross-sections was shown to have negligible impact upon the resulting mole fraction time-histories.

## 4. Experimental details

Experiments on 1-butene utilized two shock tubes, with temperatures ranging from 940 and 1440 K, pressure from 1.5 - 2.2 atm, and concentrations varying between 3-5% 1-butene in a bath gas of argon.Self-consistenttemperature trends were observed for all absorbance measurements. Example absorbance traces for 3.283 µm and 10.532 µm are presented in Fig. 2(a) and (b), respectively. Test times across both shock tube facilities were 2ms consistently. The colored data of Fig. 2were further processed to only include information after time-zero and to discount data corrupted by strong beam steering and diaphragm pieces across the beam path.
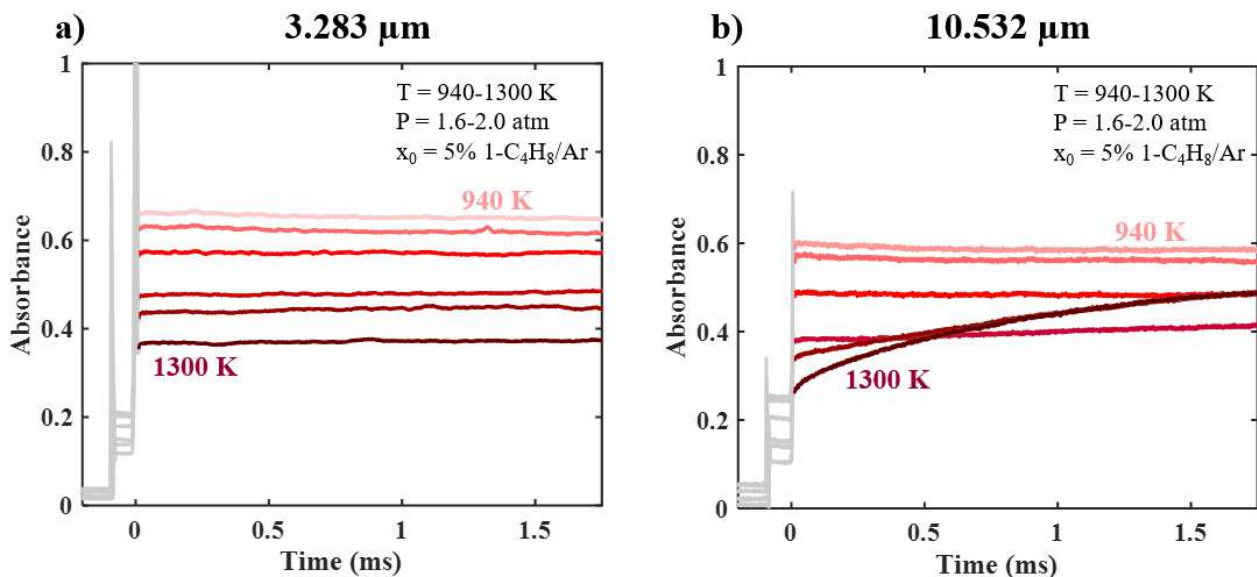
Fig. 2. Representative absorbance measurements at (a) 3.283 µmand (b) 10.532 µm of 5% 1-butene in argon at temperatures of 940 K,946 K,1028 K,1116 K, 1220 K,1300 K.

Data were collected across a span of temperatures for each wavelength of interest to facilitate the development of cross-section correlations. 1-butene pyrolysis was studied at the commoncondition of 1300 K and 1.8 atm. To study1-butene pyrolysis at a common condition across all measurements, absorbance data for each wavelength was normalized by pressure and path length and interpolated to produce an approximate absorbance trace at the desired temperature. Uncertainty associated with the interpolation process was mitigated by the use of large number of shock tube measurements very close to 1300 K and 1.8 atm.

5. Results and discussion

5.1. Laser absorbance traces

239   Fig. 3 shows pressure- and path length-normalized absorbance time-histories across the nine selected

240   wavelengths during 5% 1-butene/Ar pyrolysis at 1300 K and 1.8 atm. Individual pressure measurements

241   ranged from 1.73-1.85 atm across the experimental domain. For 8 of the 9 wavelengths, the direct output

242   of the interpolated data could be used. However, the absorbance at 10.675 µm was fitted to a double

243   exponential due to low-frequency experimental noise introduced by changes in the density (and therefore

244   refractive index) of the sample gas. Data was cropped from the absorbance time-history at 10.958 µm

245   between 1.5 and 1.75 ms, where the passage of a diaphragm piece created a large deviation in the rise

246   profile.
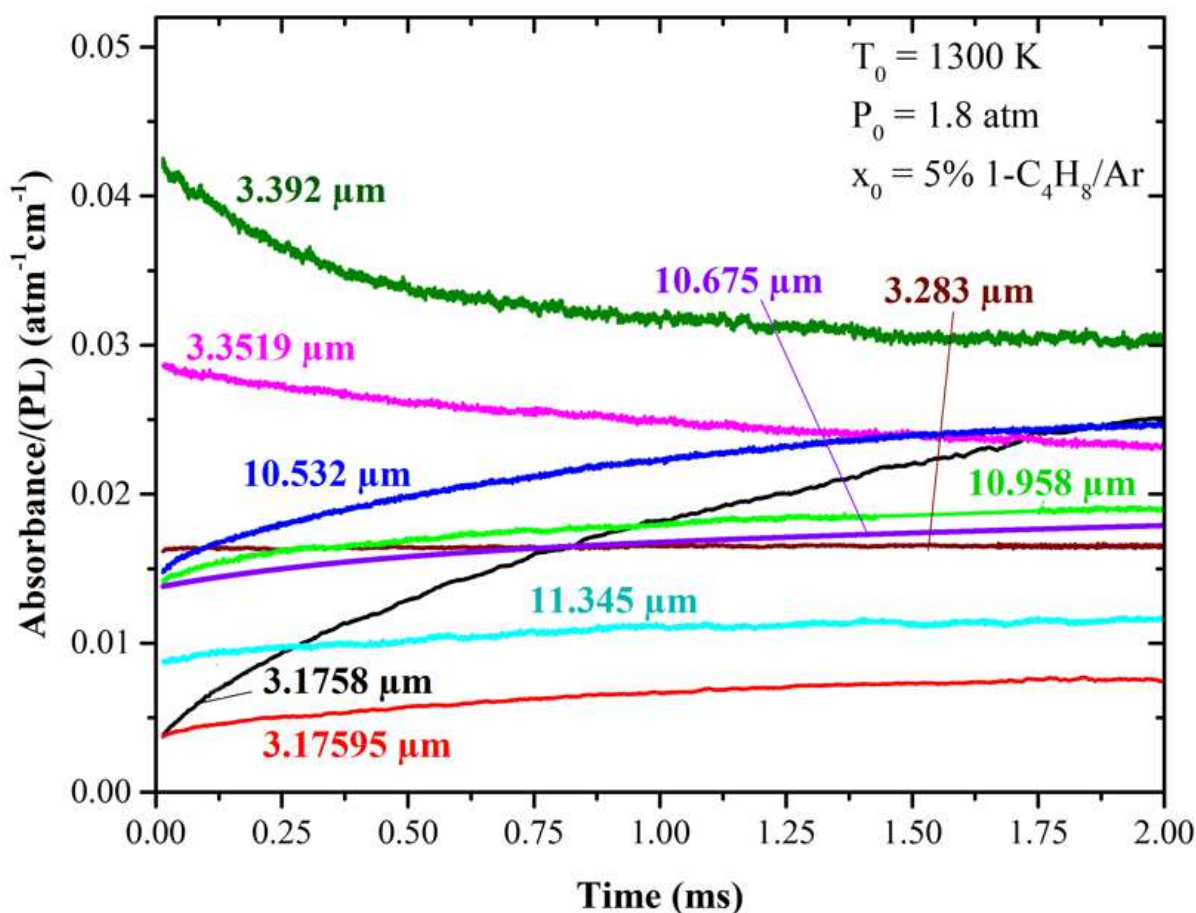
247

248   **Fig. 3.** Pressure- and pathlength-normalized absorbance traces produced at 1300 K through an

249   interpolation of shock tube measurements near 1300 K.

250

5.2. Time-resolved mole fractionsinferred during 1-butene pyrolysis

252
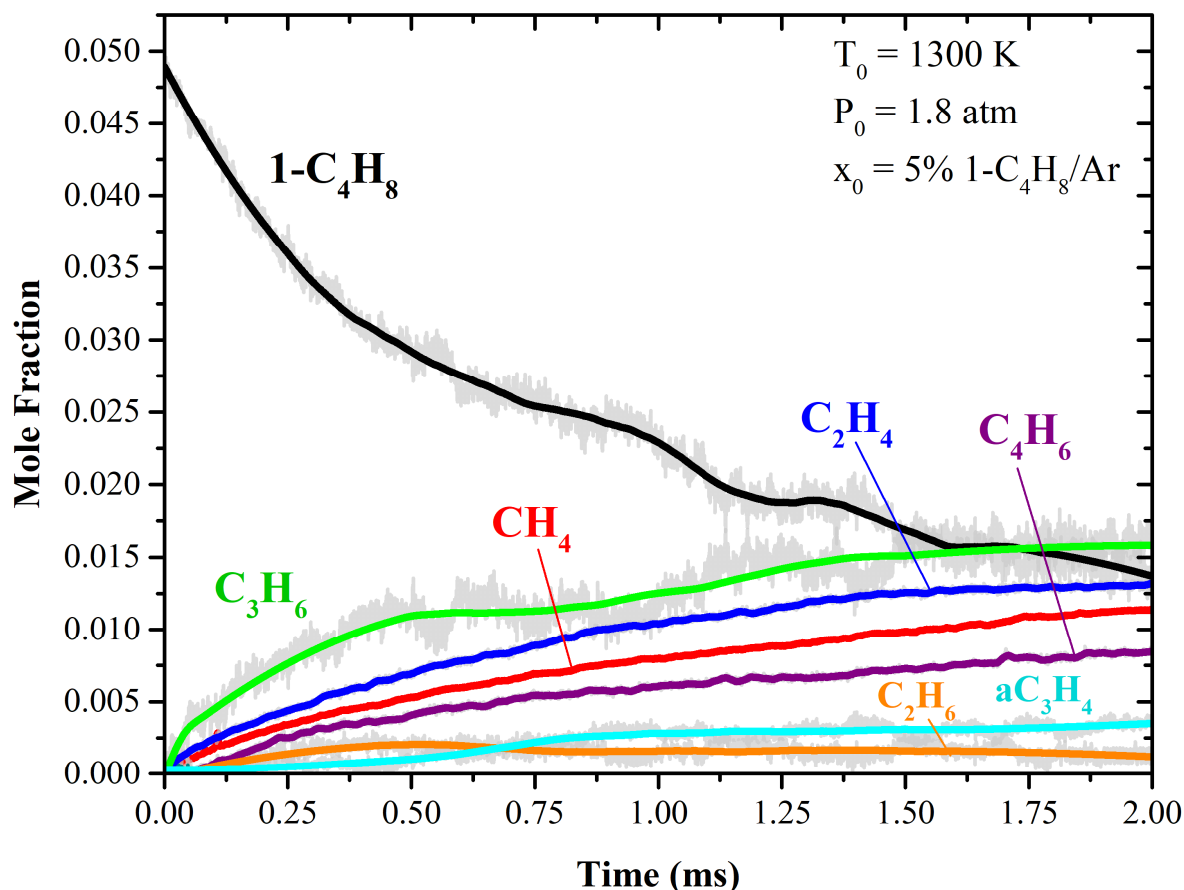
253

254

255 **Fig. 4.** Inferred mole fractions of CH_4, C_2H_4, C_2H_6, C_3H_6, aC_3H_4 (allene), $1-C_4H_8$, C_4H_6 (1,3-butadiene),

256 C_5H_6 (cyclopentadiene), and C_6H_6 from shock tube measurements of 5% $1-C_4H_8$ in argon at constant

257 pressure and an initial temperature of 1300 K.No appreciable amounts of C_6H_6,or C_5H_6weredetected.

258

259 Mole fractions werecalculated by applying the convex speciation framework to the absorbance data

260 of Fig. 3 using the database of absorption cross-section correlations presented in [21] and supplemented

261 here. Example results are shown in Fig. 4. At each instant in time, the convex system of absorbance

262 measurements and cross-section correlations was solved using the CVX software through Matlab. The

263 three constraints of Eq. 3were applied to the solution space at all times. The carbon and hydrogen

264   balance required calculation of the number of the moles in the system,which was estimated from a

265   balance of inert argon using Eq. 4.

$$\widehat{N}_t = \left(\frac{x_{0,Ar}}{\hat{x}_{t,Ar}}\right) N_0$$

(4)

266    $\widehat{N}_t$ and $\hat{x}_{t,Ar}$ are predictions of the total number of moles and mole fraction of argon at time t, and

267   N_0, $x_{0,Ar}$ are the total number of moles and mole fraction of argon at time-zero. The time-dependent

268   mole fraction of argon was estimated using Eq. 5, assuming the majority of species weremeasured.

269

$$\hat{x}_{t,Ar} \approx 1 - \sum_{i=1}^{N} x_i$$

(5)

270   Because minor species were discounted when estimating the mole fraction of argon, the calculated

271   total number of moles in the system ($\widehat{N}_t$) may slightly underestimate the true molar sum (N_t). However,

272   this systematic error serves to under-constrain, rather than artificially over-constrain, the atomic

273   conservation condition. Nevertheless, because all major species were measured, this method is expected

274   to yield accurate estimates.

275   The solution for mole fractions showed a propensity to fill the hydrogen constraint completely and

276   leave nearly 4% carbon free. Without accounting for hydrogen formation, the optimized solution was

277   found toartificially prefer speciescharacterized by ahigh hydrogen-to-carbon ratio. Because we cannot

278   measure hydrogen spectroscopically in the infrared region, a simulated hydrogen profile was used to

279   account for the hydrogen time-history in the system. The Wang et al. and Zhang et al. kinetic models are

280   in excellent agreement with respect to hydrogen formation. Therefore, to fulfill a physicallyvalid

281   hydrogen balance, hydrogen formation was simulated as the average time-historybetween the two

282   models.The free hydrogen and carbon in the systemwere also constrained with a carbon-to-hydrogen

283   ratio consistent with that of expected minor species.

284

5.2.1. Temperature dependence of the absorption cross-sections

286

The temperature dependence of the individual absorption cross-section correlations requiredspecification of the temperature profile during the endothermic pyrolysis process. Commonly, a modeled temperature profile is used in speciation[15,17,19,38,39], and the same approach isused in the current study. Amodeled temperature profilewas produced by averaging thepredictions of the Zhang et al. [30] and Wang et al. [22]mechanisms, which differ by a maximum of only 5 K at any time. All kinetic modeling was conducted at constant pressure, which wassupported by experimental measurements.Ultimately, perturbing temperature in the uncertainty analysis indicated a low sensitivity to the chosen temperature profile.

295

5.3. Weighted objective function

297

Minor and unaccounted species are expected to be present in the system in onlytrace amounts,yet their sum can constitute a substantial total. Candidate interfering species include: 2-butene, propane, propyne, pentene, toluene, and xylenes.Thesespecies created interfering absorbance that increased as a function of timeand affectedeach of the nine wavelengths differently.Due to the wavelength dependency of the interference, the system was found to beunavoidably heteroscedastic (characterized by non-uniform variability), and hencea standard least-squares cost function was deemed inappropriate. As standard in heteroscedastic systems,the weighted cost function presented in Eq. 6 was used.

305

$$Minimize \left\| W(k\vec{x} - \vec{b}) \right\|_2^2 \tag{6}$$

306

307 The matrix $\{W \in \mathbb{R}^{M \times N} \mid W_{ij} = 0 \; if \; i \neq j \; and \; 0 \leq W_{ii} \leq 1 \; \forall \, i \in \{1,2,\ldots,M\}\}$ was chosen to distribute

308 the squared errorevenly across all wavelengths,despitethe presence of interfering species. Weights were

309 selected based on best approximations of the spectra of minor species. The procedure for setting the

310 maindiagonal of matrix $W$was: (1)candidate interferers were determined using flow reactor data and

311 existing kinetic mechanisms from the literature, (2) where possible, a composite spectrum of the

312 predicted interfering species was generated using low-temperature FTIR data, (3) the combined spectra

313 were used to create a vector ranging from 0 to 1 that indicated the strength of the interference spectrum

314 at each wavelength, and (4) atime-history was generated that decayed from one to$(1 - \text{strength})$that

315 followed the system rise-time. The system rise-time was determined from the 10.532 µm absorbance

316 trace.At each instant in time, the elements of the main diagonal of matrix Wwere set using the time-

317 histories of (4) at each associated wavelength. Ultimately, the recovered time-histories of most species

318 proved relatively insensitive to the individual weights applied. Numerical perturbation of the weighting

319 structure factors into the measured uncertainty of each species recovered.

320

321 *5.4. Uncertaintyquantification*

322

323   Uncertainty was propagated through numerical perturbation of the cross-section correlations,

324 absorbance measurements, and temperature. The uncertainty,u, of species i at time $t$was calculated to

325 one standard deviationusing Eq. 7,assuming that uncertainty in the absorption cross-sections,

326 absorbance, and the temperature dominate.

327

$$u_i(t) = \sqrt{\sum_{j=1}^{M}\sum_{k=1}^{N}\left(\frac{\partial x_i}{\partial \sigma_{j,k}}\right)^2 \delta\sigma_{j,k}^2 + \sum_{j=1}^{M}\left(\frac{\partial x_i}{\partial b_j}\right)^2 \delta b_j^2 + \sum_{j=1}^{M}\left(\frac{\partial x_i}{\partial W_j}\right)^2 \delta W_j^2 + \left(\frac{\partial x_i}{\partial T}\right)^2 \delta T^2} \qquad (7)$$

328 $\left(\frac{\partial x_i}{\partial \sigma}\right)$, $\left(\frac{\partial x_i}{\partial b}\right)$, $\left(\frac{\partial x_i}{\partial W}\right)$, and $\left(\frac{\partial x_i}{\partial T}\right)$ are computed numerical derivatives of the mole fraction of species x_i

329 with respect to the cross-section correlation σ, normalized absorbance b, weight W, and the temperature

330 T. $\delta\sigma$, δb, δW, and δT are the associated uncertainties of the cross-sections, normalizedabsorbance,

331 weights, and thetemperature to one standard deviation. The cross-sections uncertaintieswere calculated

332 using the parameters in Table 2 and[21] using the method describedin[21].$\delta b$was estimated by

333 propagating uncertainty through the Beer-Lambert relation with contributions from path length, pressure,

334 and intensities$I$ and I_0. Notably, the uncertainty associated with the attenuated intensity$I$was found to be

335 the dominant source of uncertainty in the absorbance time-histories. Uncertainty in the weights was

336 taken as $\delta W = 0.1$. Uncertainty in temperature is conservatively estimated by $\delta T = 20$ K, which is four

337 times larger than the largest temperature difference between the two models. The measured mole

338 fractions including their uncertaintiesare presented in Fig. 5 to one standard deviation.

339
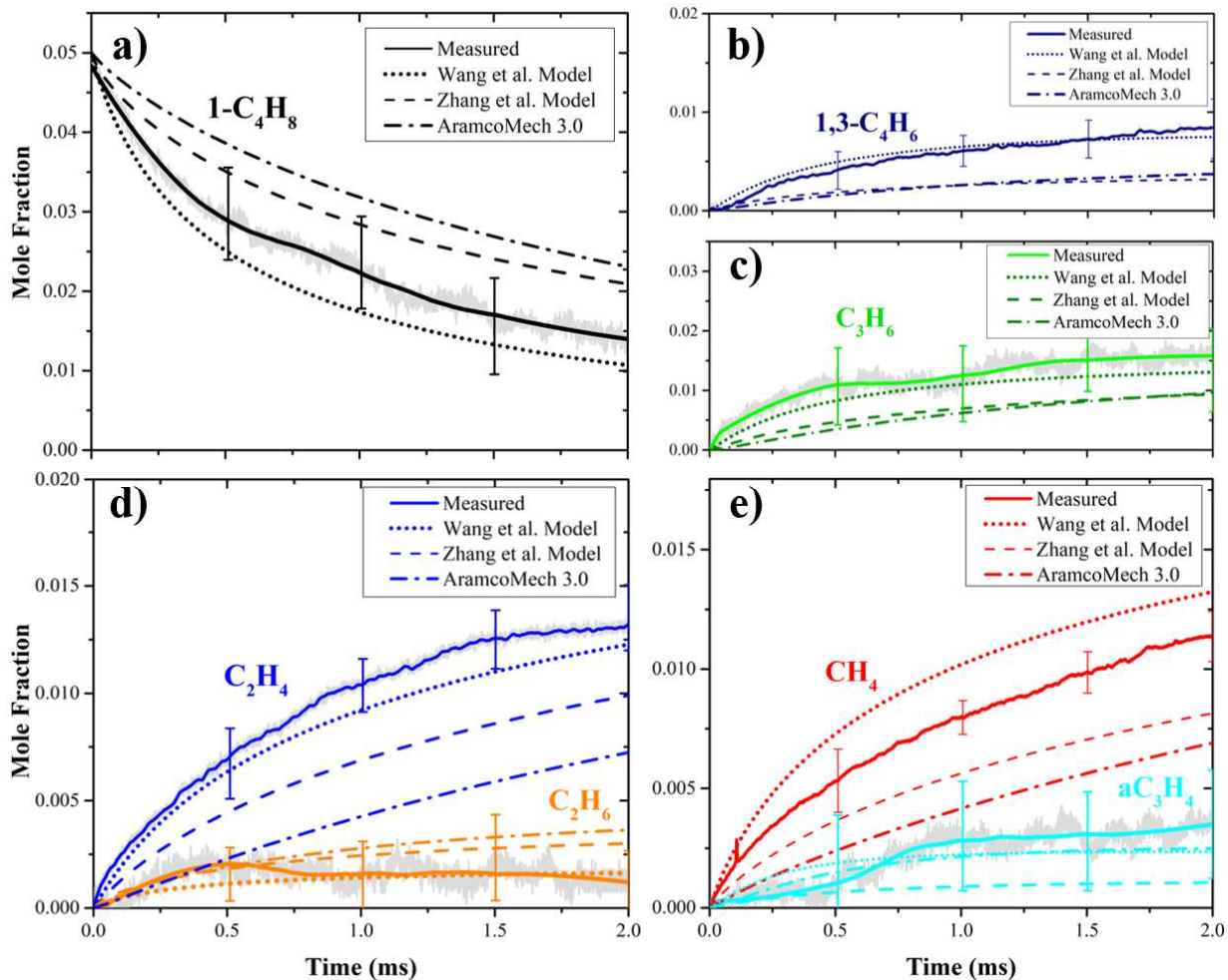
Fig. 5. Measured mole fractionsversus time in comparison to two 1-butene-specific kinetic models, from Wang et al. [22]and Zhang et al. [30],and also the AramcoMech 3.0 model[40]for (a) 1-butene (b) 1,3-butadiene (c) propene (d) ethylene and ethane, and (e) methane andallene.Error bars represent 1-sigma uncertainty.

The inferred mole fractions and their uncertainties were compared to two 1-butene specific models, the work of Wang et al. [22] and Zhang et al. [30], as well as the Aramco 3.0 kinetic model[40]. Across all species, the measured mole fractions were found to be in good agreement with the predictions of the Wang et al. kinetic model. Two species, 1-butene and methane, were exceptions. They were observed to react at a slower rate than Wang et al. but a faster rate than the Zhang et al. model. For the majority of

351 species, such as ethylene, 1,3-butadiene, propene, ethane, and allene, the predictions of Wang et al. were

352 well within the experimental uncertainties of the measurements. Comparisons were also drawn

353 againstthe AramcoMech 3.0 kinetic modeland are shown in Fig. 5. A difference in 1-butene

354 decomposition rate was observed between the measured and AramcoMech 3.0 predictions.

355 Consequently,the formation rate of major speciessuch as ethylene, propene, methane, and 1,3-butadiene

356 are predicted to be slower than experimentally measured. Strong agreement exists between AramcoMech

357 3.0 and the inferred mole fraction of allene.

358 Within the sensitivity of the current method, only trace amounts of benzene and cyclopentadiene

359 were detected. However, through the uncertainty analysis, valuable insights can be garnered about

360 cylcopentadiene and benzene in comparison to the existing kinetic models, as shown in Fig. 6 (a-b).

361 Concerning cyclopentadiene, the uncertainty bounds for the current method indicate agreement between

362 the inferred mole fractions and the predictions of Wang et al. and AramcoMech 3.0; however, no such

363 agreement exists in comparison to the Zhang et al. mechanism. No appreciable amount of benzene was

364 detected in the current method, yet the measurement uncertainty encompasses the small amounts of

365 benzene predicted from all models. More fixed-wavelength lasers could be added in order to increase

366 measurement sensitivity and decrease uncertainty for trace species.
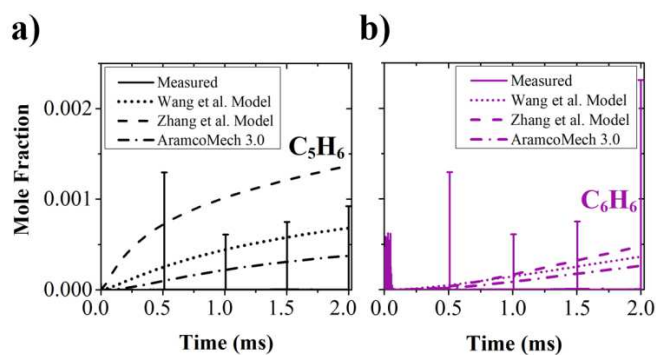
368 **Fig. 6.** Measured mole fractions versus time for (a) cyclopentadiene and (b) benzene in comparison to

369 two 1-butene specific kinetics models, from Wang et al. [22] and Zhang et al. [30], and also the

370 AramcoMech 3.0 model[40]. A shared ordinate axis is provided and is notably limited to a mole fraction

371 value of only 0.0025.
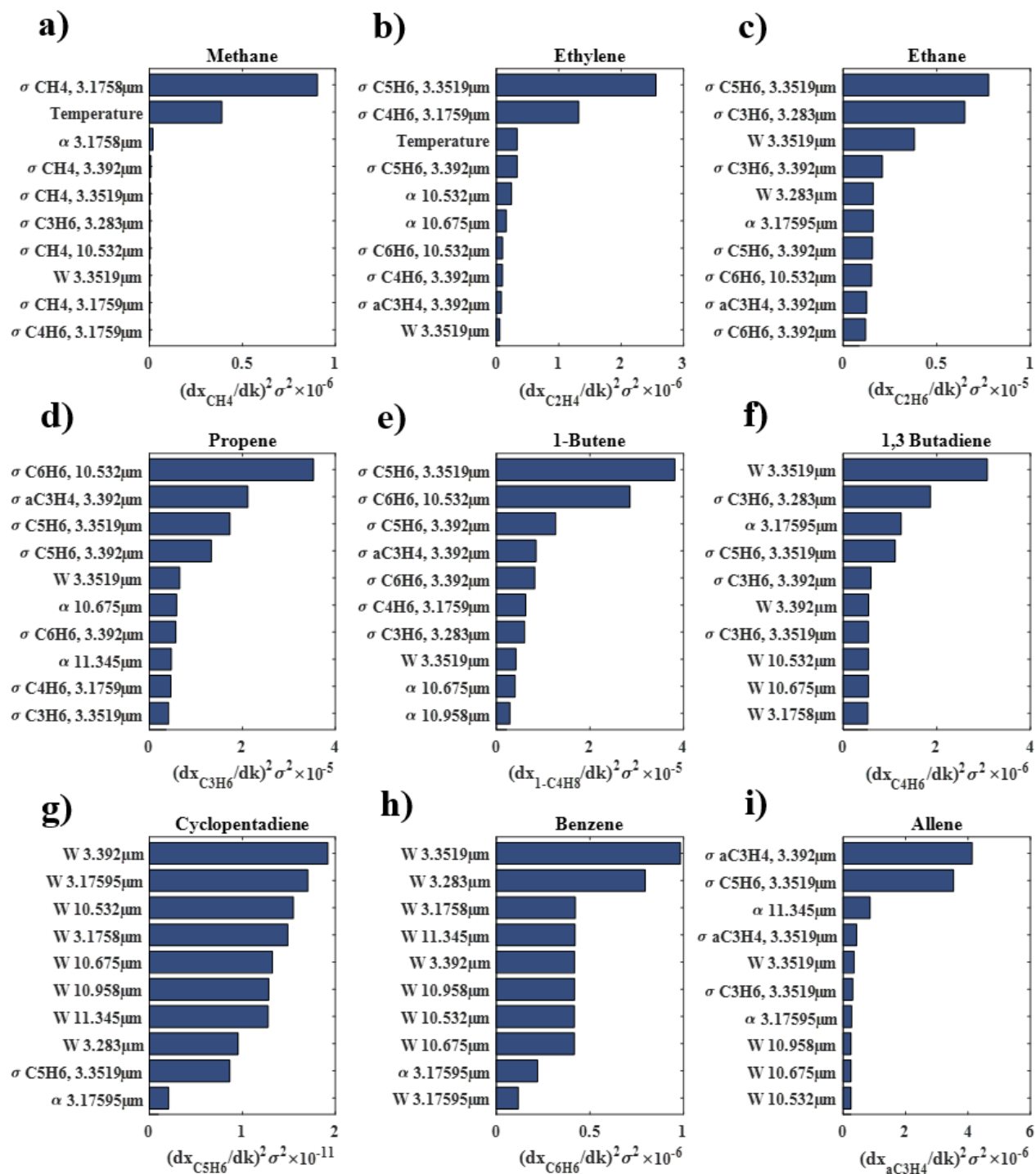
Fig. 7. The top 10squared uncertainty contributionsfrom cross-sections (σ), absorbance measurements(α), temperature, and weight parameter (W)on each speciesmole fraction at 2 ms for (a)

376   methane, (b) ethylene, (c) ethane, (d) propene, (e) 1-butene,(f) 1,3-butadiene,(g) cyclopentadiene, (h)

377   benzene, and (i) allene.(dx_i/dk) refers to the derivative of the mole fraction with respect to each

378   variable of interest (k indicates eitherσ, α, T, or W).

379

380   In order to identify system parameters for which reduced uncertainty is desired, the measurement

381   uncertainty associated with each cross-section, absorbance, weight, and the temperature profile were

382   evaluated and compared across all species. It was found that a few cross-section correlations were

383   responsible for the majority of the uncertainty in the system. Accordingly, cross-section correlations with

384   the largest contribution to the system uncertainty were identified as prominent targets for future research

385   and cross-section database refinement. Specifically, these include cross-sections of minor species such as

386   benzene and cyclopentadiene. Anuncertainty evaluation is presented in Fig.7 to indicate the 10 system

387   parameters contributing the largest uncertainties to the measured mole fractions ofthe nine species

388   included in the absorption cross-section matrix. Evident in Fig. 7 are the sensitivities to the cross-

389   sections of minor species and the relative insensitivity to the system-weighting parameters for all

390   species. Although weighting parameters appear prominently in the sensitivities of benzene and

391   cyclopentadiene, these species are present in such trace amounts thatthey cause no significant change in

392   the measured mole fractions of other reported species. Recommended future studies include further

393   absorption cross-section measurements of cyclopentadiene at 3.3519 µm, propene at 3.283 µm, and

394   allene at 3.392 µm.

395

396   **6.   Conclusion**

397

398   In the first demonstration of the laser absorption spectroscopy matrix speciation method proposed in

399   [21], shock tube time-histories of nine wavelengths were used to resolve species mole fractions during

400   the high-temperature pyrolysis of 1-butene. Because ethane was predicted to be an important pyrolysis

401   product, a new wavelength at 3.3519 µm, sensitive to ethane absorption, was developed. This

402   wavelength, along with eight additional wavelengths in the 3 – 4 µm and 10 – 11 µm regions, were used

403   to simultaneously solve for the time-histories of 1-butene, methane, ethylene, ethane, allene, propene,

404   1,3-butadiene, benzene, and cyclopentadieneduring 5% 1-butene decomposition in argon at shock tube-

405   generated conditions of 1300 K and 1.8 atm. To resolve the contributions of each species to each

406   wavelength, new cross-sections of relevant species were measured to supplement an existing database of

407   cross-section correlations.Overall, the resulting time-histories show good agreement with existing kinetic

408   models developed for 1-butene, especially the model proposed by Wang et al. [22]. Because the

409   pyrolysis offuels has been found to play an important role in their combustion pathways, the matrix

410   speciation method demonstrated here can be a useful tool in uncovering fueldecomposition behavior at

411   the short timescales relevant to combustion. With additional carefullychosen wavelengths to resolve

412   additional species, this framework can be readily extended from 1-butene to a range of more complex

413   hydrocarbon fuels with direct aerospace and automotive applications.

414

415   **Appendix A: Sensitive ethane wavelength selection**

416

417   *A.1. Survey of ethane absorption spectrum*

418

419   Selecting a wavelength for species-specific measurements requires consideration both of target- and

420   interfering-species absorption, as well as the availability of narrow-linewidth, continuous-wave lasers.

421   Generally, because a single-wavelength diagnostic cannot distinguish between absorption from different

422   species, substantial weight is placed on the interference-free criterion in selecting diagnostic lines.

423   Hence, the wavelength selected for ethane detection was intentionally chosen for use in a multi-

424   wavelength speciation method. Within this framework, although freedom from interference is preferred,

425   strict isolation from interfering species is not required. Rather, a wavelength was chosen at which

426   absorbance has unique sensitivity to the presence of ethane in the system. Put differently, the additional

427 wavelength was selected to provide a distinct vector of cross-sections that enables more robust detection

428 of all species, but especially ethane.

429
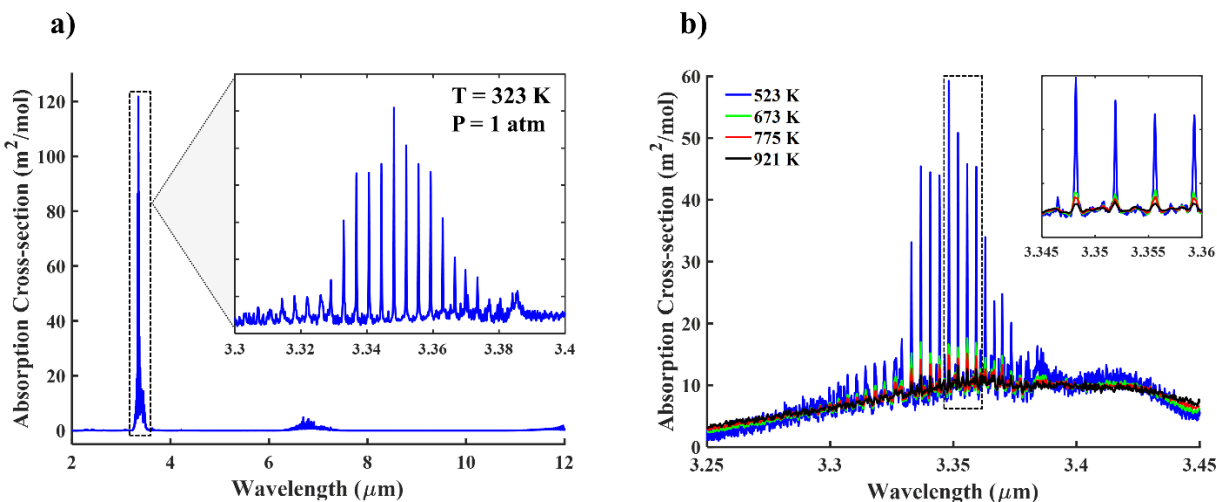
430

431

432 **Fig. A.1**. (a) PNNL-measured infrared absorption spectrum for ethane [41], and (b) KAUST-measured

433 ethane spectra at elevated temperatures [27]. The 3.3 µm region offers the strongest IR absorption, with

434 narrow Q-branches collapsing into a broadband high-temperature feature.

435

436   Fig. A.1(a) shows the infrared spectrum of ethane at 323 K measured by Pacific Northwest National

437 Laboratory (PNNL) [41]. Strong absorption in the 3 µm mid-infrared (MIR) region arises from multiple

438 fundamental CH_3 stretch modes (ν_5 and ν_7) as well as numerous combination bands [42]. Although this

439 region fortuitously coincides with compact, commercially available MIR lasers, it is also a common

440 region of absorption for virtually all hydrocarbons. Such crowded absorption necessitates judicious

441 wavelength selection to mitigate interference and optimize ethane sensitivity. Fig. A.1(b) gives a closer

442 view of the 3 µm ethane spectrum at increasing temperatures, measured by KAUST with a Fourier

443 transform infrared spectrometer (FTIR) [27]. The strong, narrow peaks correspond to Q-branches of the

444 ν_7 fundamental.   As temperature increases, these structured features give way to the broadband

445 absorption of many closelyspaced hot band transitions. That ethane behaves spectrally like a small

446   molecule (structured) at low temperatures and a large molecule (broadband) at high temperatures

447   complicates the line-selection process by eliminating the possibility of an online/offline measurement

448   technique in high-temperature shock tube experiments. Nevertheless, a well-chosen wavelength with

449   minimal interference can yield sensitive ethane detection in a multi-wavelength, multi-species

450   measurement approach.

451

452   *A.2. Wavelength selection*

453

454   Because of its strong absorption and commercial laser accessibility, the 3.3 µm region was chosen as

455   the preferred spectral location for ethane sensing. Within this region, a systematic search was

456   undertaken for the optimal combination of strong absorption and relative freedom from interference over

457   a broad range of experimental conditions. In conducting the search, FTIR cross-section data from

458   KAUST [27,43] and Klingbeil et al. [44]werecombinedwith line listsfrom HITRAN 2016 [45] to predict

459   absorption from ethane and interferers methane, ethylene, acetylene, propene, and 1-butene. It should be

460   noted that the HITRAN line list is incomplete and primarily tabulates Q-branch transitions in the 3.3 µm

461   region. It does not capture the large broadband absorbance that surrounds the Q-branch peaks but does

462   yield reasonable predictions for the behavior of these peaks at the high temperatures of interest.

463   Using both FTIR cross-section data and HITRAN simulations, the 3.3 µm – 3.4 µm region was

464   searched for a stronglyabsorbing, interference-mitigating ethane wavelength. The wavelengths

465   corresponding to Q-branch peaks were specifically studied for their favorable absorbance across a broad

466   range of temperatures and pressures. Because both ethane and larger interfering species become

467   relatively smooth at high temperatures, particular attention was paid to interference from discrete small-

468   molecule transitions, namely those of methane and ethylene. Ultimately, 3.35191 µm was chosen as the

469   preferred wavelength with which to measure ethane. Fig. A.2 shows ethane cross-sections overlaid with

470   those of 1-butene, propene, methane, and ethylene at selected high temperatures where data exist. A

471   vertical line indicates the target wavelength selection. At this chosen wavelength, the advantageous

472 combination of strong ethane cross-section with only weak interference from methane and ethylene is

473 evident. While 1-butene and propene have large cross-sections across the entire candidate region, their

474 contributions to measured absorbance were accounted for by the multi-wavelength measurement strategy

475 employed here.

476
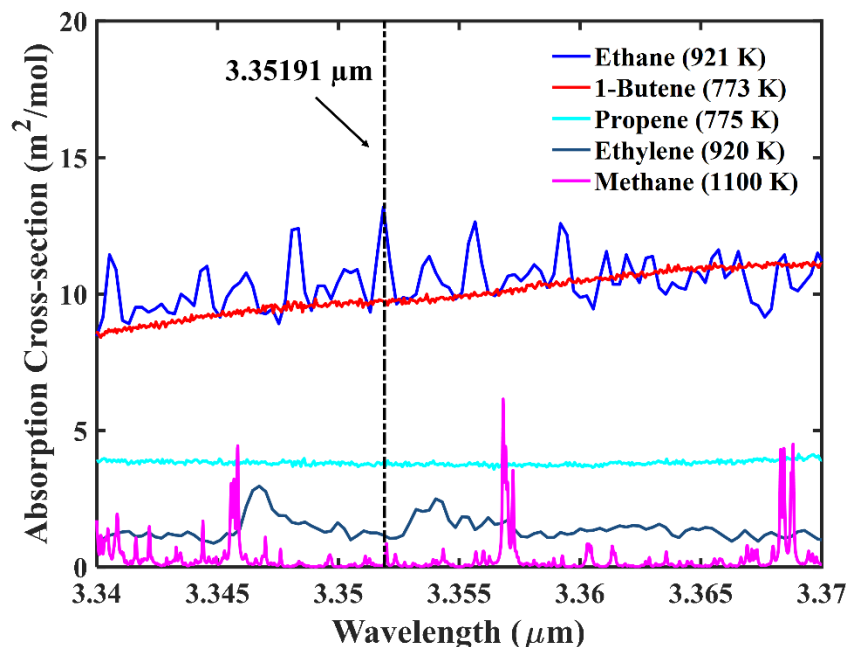
477

478

479 **Fig. A.2**. Ethane cross-sections compared with interference from 1-butene, propene, ethylene, and

480 methane at 1 atm. The chosen wavelength for ethane detection, 3.35191 µm, is shown as a vertical line.

481 Methane interference was simulated with HITRAN 2016 [45], while ethane [27], 1-butene [44], propene

482 [44], and ethylene [27] cross-sections were taken from FTIR-measured literature data.

483

484 **Appendix B: Multi-wavelength cross-section matrix**

485

486 The majority of the absorption cross-section correlations and associated uncertainty directly

487 reference Pinkowski et al. [21], but a large number of new correlations were required for ethane, 1,3-

488 butadiene, cyclopentadiene, and allene. Table B.1 presents a visualization of the absorption cross-

489 section matrix used in this work. Cross-sections from the literature appear in gray and new cross-

490 sections from shock tube measurements are shown in white. Table B.2 presents these new cross-section

491 correlations for individual species and wavelengths. Fig. B.1 shows the experimental data supporting the

492 correlations of Table B.2. In certain cases where absorption cross-sections were unavailable,

493 approximations are reported from extrapolations of available FTIR and broadlytuned laser [46] data.

494 Nonetheless, the pyrolysis time-histories reported here were shown to be insensitive to these few

495 approximated cross-sections.

496

497 **Table B.1**. Cross-section matrix used for 1-butene speciation. Gray cells reference cross-sections
498 published previously in the literature. White cells indicate new cross-section correlations.

Wavelength	CH_4	C_2H_4	C_2H_6	C_3H_6	aC_3H_4	$1C_4H_8$	C_4H_6	C_5H_6	C_6H_6
3.1758μm	$\sigma_{1,1}$	$\sigma_{1,2}$	$\sigma_{1,3}$	$\sigma_{1,4}$	$\sigma_{1,5}$	$\sigma_{1,6}$	$\sigma_{1,7}$	$\sigma_{1,8}$	$\sigma_{1,9}$
3.17595μm	$\sigma_{2,1}$	$\sigma_{2,2}$	$\sigma_{2,3}$	$\sigma_{2,4}$	$\sigma_{2,5}$	$\sigma_{2,6}$	$\sigma_{2,7}$	$\sigma_{2,8}$	$\sigma_{2,9}$
3.283μm	$\sigma_{3,1}$	$\sigma_{3,2}$	$\sigma_{3,3}$	$\sigma_{3,4}$	$\sigma_{3,5}$	$\sigma_{3,6}$	$\sigma_{3,7}$	$\sigma_{3,8}$	$\sigma_{3,9}$
3.3519μm	$\sigma_{4,1}$	$\sigma_{4,2}$	$\sigma_{4,3}$	$\sigma_{4,4}$	$\sigma_{4,5}$	$\sigma_{4,6}$	$\sigma_{4,7}$	$\sigma_{4,8}$	$\sigma_{4,9}$
3.392μm	$\sigma_{5,1}$	$\sigma_{5,2}$	$\sigma_{5,3}$	$\sigma_{5,4}$	$\sigma_{5,5}$	$\sigma_{5,6}$	$\sigma_{5,7}$	$\sigma_{5,8}$	$\sigma_{5,9}$
10.532μm	$\sigma_{6,1}$	$\sigma_{6,2}$	$\sigma_{6,3}$	$\sigma_{6,4}$	$\sigma_{6,5}$	$\sigma_{6,6}$	$\sigma_{6,7}$	$\sigma_{6,8}$	$\sigma_{6,9}$
10.675μm	$\sigma_{8,1}$	$\sigma_{8,2}$	$\sigma_{8,3}$	$\sigma_{8,4}$	$\sigma_{8,5}$	$\sigma_{8,6}$	$\sigma_{8,7}$	$\sigma_{8,8}$	$\sigma_{8,9}$
10.958μm	$\sigma_{9,1}$	$\sigma_{9,2}$	$\sigma_{9,3}$	$\sigma_{9,4}$	$\sigma_{9,5}$	$\sigma_{9,6}$	$\sigma_{9,7}$	$\sigma_{9,8}$	$\sigma_{9,9}$
11.35μm	$\sigma_{10,1}$	$\sigma_{10,2}$	$\sigma_{10,3}$	$\sigma_{10,4}$	$\sigma_{10,5}$	$\sigma_{10,6}$	$\sigma_{10,7}$	$\sigma_{10,8}$	$\sigma_{10,9}$

499

500

501

502

503

504

505

506

507   **Table B.2.** Cross-section correlation table for new correlations.

Species	Cell	Fitted value of cross-section $(\sigma \, [\frac{m2}{mol}])$ vs. temperature $(T \, [K])$ in	Standard error $(n = \# \, of \, samples)$	Reference	Notes and literature correlations
Cross-sections at 3.1758 μm					
C_2H_6	1,3	$\sigma = a_0 + a_1 T$ $a_0 = 0.14548$ $a_1 = -3.37354E - 5$	$n = 30$ $\nu = 28$ $RSS = 0.05137$ $t_{95} = 2.048$ $s_{TT} = 3.68E6$ $\bar{T} = 1109.078$	New	Correlation valid between 300-1300 K.
aC_3H_4	1,5	Approximately zero		[37,41]	Approximately zero.
C_4H_6	1,7	$\sigma = a_0 + a_1 T$ $a_0 = 0.98562$ $a_1 = -2.1536E - 4$	$n = 6$ $\nu = 4$ $RSS = 0.04421$ $t_{95} = 2.776$ $s_{TT} = 5.3E5$ $\bar{T} = 1067.676$	New	Correlation valid between 700-1550 K.
C_5H_6	1,8	$\sigma = a_0 + a_1 T$ $a_0 = 0.10094$ $a_1 = 4.5048E - 5$	Approximation	Approximation	Assumed to be ¼ the absorption cross-section as 3.392 μm. Low absorption cross-section expected.
Cross-sections at 3.17595 μm					

C_2H_6	2,3	$\sigma = a_0 + a_1 T$ $a_0 = 0.14548$ $a_1 = -3.37354E-5$	$n = 30$ $v = 28$ $RSS = 0.05137$ $t_{95} = 2.048$ $s_{TT} = 3.68E6$ $\bar{T} = 1109.078$	*New*	*Assumed to be the same as 3.1758 μm. Correlation valid between 300-1300 K.*
aC_3H_4	2,5	*Approximately zero*		[37,41]	*Approximately zero.*
C_4H_6	2,7	$\sigma = a_0 + a_1 T$ $a_0 = 0.98562$ $a_1 = -2.1536E-4$	$n = 6$ $v = 4$ $RSS = 0.04421$ $t_{95} = 2.776$ $s_{TT} = 5.3E5$ $\bar{T} = 1067.676$	*New*	*Assumed to be the same as 3.1758 μm. Correlation valid between 700-1550 K.*
C_5H_6	2,8	$\sigma = a_0 + a_1 T$ $a_0 = 0.10094$ $a_1 = 4.5048E-5$	*Approximation*	*Approximation*	*Assumed to be ¼ the absorption cross-section at 3.392 μm. Low absorption cross-section expected.*
Cross-sections at 3.283 μm					
C_2H_6	3,3	$\sigma = a_0 + a_1 T + a_2 T^2$ $a_0 = 2.08095$ $a_1 = -0.00203$ $a_2 = 5.35068E-7$	$n = 39$ $v = 36$ $RSS = 0.1843$ $t_{95} = 2.042$ $s_{TT} = 4.21E6$ $\bar{T} = 1101.33$	*New*	*Correlation valid between 600-1800 K.*
aC_3H_4	3,5	*Approximately zero*		[37,41]	*Approximately zero.*
C_4H_6	3,7	$\sigma = a_0 + a_1 T + a_2 T^2$ $a_0 = -0.46373$ $a_1 = 0.00719$ $a_2 = -3.13536E-6$	$n = 6$ $v = 3$ $RSS = 0.01955$ $t_{95} = 3.182$ $s_{TT} = 5.30E5$ $\bar{T} = 1067.676$	*New*	*Correlation valid between 700-1550 K.*

C_5H_6	3,8	$\sigma = a_0 + a_1 T$ $a_0 = 0.40375$ $a_1 = 1.8019E-4$	*Approximation*	*Approximation*	*Assumed to be the same as the absorption cross-section at 3.392μm. Low absorption cross-section expected.*
Cross-sections at 3.3519 μm					
CH_4	4,1	$\sigma = a_0 + a_1 T + a_2 T^2$ $a_0 = -3.88202$ $a_1 = 0.00861$ $a_2 = -2.79276E-6$	$n = 16$ $\nu = 13$ $RSS = 0.65252$ $t_{95} = 2.160$ $s_{TT} = 2.64E6$ $\bar{T} = 1214.97$	*New*	*Correlation valid between 600-2100 K.*
C_2H_4	4,2	$\sigma = a_0 + a_1 T + a_2 T^2$ $a_0 = 0.79448$ $a_1 = 5.36859E-4$ $a_2 = -2.13847E-7$	$n = 8$ $\nu = 5$ $RSS = 0.02818$ $t_{95} = 2.571$ $s_{TT} = 1.43E6$ $\bar{T} = 1214.7$	*New*	*Correlation valid between 700-2000 K.*
C_2H_6	4,3	$\sigma = a_0 + a_1 \exp\left(-\dfrac{T - x_0}{b_1}\right)$ $a_0 = 4.03848$ $a_1 = 47.26708$ $b_1 = 679.65013$ $x_0 = 251.60459$	$n = 28$ $\nu = 24$ $RSS = 709.4$ $t_{95} = 2.064$ $s_{TT} = 3.79E6$ $\bar{T} = 1156.89$	*New*	*Correlation valid between 600-2000 K. Slight pressure dependence observed below 1000 K.*
C_3H_6	4,4	$\sigma = a_0 + a_1 \exp\left(-\dfrac{T - x_0}{b_1}\right)$ $a_0 = 2.5978$ $a_1 = 2.9384$ $b_1 = 343.40548$ $x_0 = 303.0564$	$n = 12$ $\nu = 8$ $RSS = 1.31982$ $t_{95} = 2.306$ $s_{TT} = 1.43E6$ $\bar{T} = 820.912$	*New &[44]*	*Correlation valid between 300-1600 K.*
aC_3H_4	4,5	$\sigma = a_0 + a_1 T + a_2 T^2$ $a_0 = 0.34$ $a_1 = 0.0012$ $a_2 = -5.7989$	*Approximation*	*[37,41]*	*Approximated as 1/3 of the absorption cross-section of 1,3-C_4H_6 based on FTIR data up to 510 K. Uncertainty estimated as 1,3-C_4H_6 uncertainty.*

$1C_4H_8$	4,6	$\sigma = a_0 + a_1T$ $a_0 = 14.91918$ $a_1 = -0.00678$	$n = 8$ $\nu = 6$ $RSS = 1.14718$ $t_{95} = 2.447$ $s_{TT} = 8.02E5$ $\bar{T} = 1020.51675$	*New*	*Correlation valid between 600-1700 K.*
C_4H_6	4,7	$\sigma = a_0 + a_1T + a_2T^2$ $a_0 = 1.02567$ $a_1 = 0.00369$ $a_2 = -1.73969E - 6$	$n = 6$ $\nu = 3$ $RSS = 0.00225$ $t_{95} = 3.182$ $s_{TT} = 5.30E5$ $\bar{T} = 1067.676$	*New*	*Correlation valid between 700-1550 K.*
C_5H_6	4,8	$\sigma = a_0 + a_1T$ $a_0 = 0.40375$ $a_1 = 1.8019E - 4$	*Approximation*	*Approximation*	*Assumed to be the same as the absorption cross-section at 3.392 µm. Low absorption cross-section expected.*
C_6H_6	4,9	*Approximately zero*	*Approximation*	[41]	*Approximately zero.*
Cross-sections at 3.392 µm					
C_2H_6	5,3	$\sigma = a_0 + a_1T$ $a_0 = 11.92392$ $a_1 = -0.00365$	$n = 16$ $\nu = 14$ $RSS = 0.46103$ $t_{95} = 2.145$ $s_{TT} = 4.37E4$ $\bar{T} = 649.15$	[28]	*Correlation valid between 300-1500 K.*
aC_3H_4	5,5	*Approximately zero*	*Approximation*	[37,41]	*Approximately zero.*
C_4H_6	5,7	$\sigma = a_0 + a_1T$ $a_0 = 1.06643$ $a_1 = 4.80739E - 4$	$n = 11$ $\nu = 9$ $RSS = 0.08677$ $t_{95} = 2.262$ $s_{TT} = 1.67E5$ $\bar{T} = 1251.222$	*New*	*Correlation valid between 1100-1500 K.*

C_5H_6	5,8	$\sigma = a_0 + a_1T$ $a_0 = 0.40375$ $a_1 = 1.8019E - 4$	$n = 25$ $\nu = 23$ $RSS = 0.18271$ $t_{95} = 2.069$ $s_{TT} = 5.87E5$ $\bar{T} = 1200.41$	*New*	*Correlation valid between 800-1600 K.*

Cross-sections at 10.532 μm

C_2H_6	6,3	*Approximately zero*	*Approximation*	[41]	*Approximately zero.*
aC_3H_4	6,5	*Approximately zero*	*Approximation*	[37,41]	*Approximately zero.*
C_4H_6	6,7	$\sigma = a_0 + a_1T$ $a_0 = 7.0509$ $a_1 = 0.001513$		[47]	
C_5H_6	6,8	$\sigma = a_0 + a_1T + a_2T^2$ $a_0 = -1.13732$ $a_1 = 0.0675$ $a_2 = -3.0986E - 6$	$n = 23$ $\nu = 20$ $RSS = 0.02439$ $t_{95} = 2.086$ $s_{TT} = 2.96E5$ $\bar{T} = 1247$	*New*	*Correlation valid between 800-1600 K.*

Cross-sections at 10.675 μm

C_2H_6	7,3	*Approximately zero*	*Approximation*	[41]	*Approximately zero.*
aC_3H_4	7,5	*Approximately zero*	*Approximation*	[37,41]	*Approximately zero.*
C_4H_6	7,7	$\sigma = a_0 + a_1T$ $a_0 = 7.0509$ $a_1 = 0.001513$		[47]	*Assumed to be the same as 10.532 μm.*
C_5H_6	7,8	$\sigma = a_0 + a_1T$ $a_0 = -1.77244$ $a_1 = 0.00415$	$n = 4$ $\nu = 2$ $RSS = 0.0262$ $t_{95} = 4.303$ $s_{TT} = 2.55E4$ $\bar{T} = 1108.9$	[47]	*Correlation valid between 800-1600 K.*

Cross-sections at 10.958 μm

C_2H_6	8,3	*Approximately zero*		[41]	*Approximately zero.*

aC_3H_4	8,5	$\sigma = a_0 + a_1T + a_2T^2$ $a_0 = 7.2996$ $a_1 = -0.00478$ $a_2 = 1.23919E-6$	$n = 5$ $v = 2$ $RSS = 0.02565$ $t_{95} = 4.303$ $s_{TT} = 3.07E5$ $\bar{T} = 1257$	[48]	*Approximated as having the same absorption at 10.958 µm as 10.962 µm due to broad features and using cross-sections measured by Chrystie et al. [48]. Correlation valid between 900-1650 K.*
C_4H_6	8,7	$\sigma = a_0 + a_1T$ $a_0 = 9.86671$ $a_1 = -0.00287$	$n = 4$ $v = 2$ $RSS = 0.37894$ $t_{95} = 4.303$ $s_{TT} = 4.12E5$ $\bar{T} = 1037$	[46,47]	*Correlation valid between 600 K and 1600 K.*
C_5H_6	8,8	$\sigma = a_0 + a_1T + a_2T^2$ $a_0 = 2.49963$ $a_1 = 0.00303$ $a_2 = -1.8117E-6$	$n = 8$ $v = 5$ $RSS = 0.00113$ $t_{95} = 2.571$ $s_{TT} = 1.31E5$ $\bar{T} = 1242$	[47]	*Correlation valid between 1000 K and 1500 K.*
Cross-sections at 11.345 µm					
C_2H_6	9,3	*Approximately zero*		[41]	*Approximately zero.*
aC_3H_4	9,5	$\sigma = a_0 + a_1T$ $a_0 = 1.9421$ $a_1 = 0.0010984$	*Approximation*	[37]	*Approximated as having absorption cross-section as 1,3-butadiene at 11.345 µm based on inspection of FTIR spectra up to 510 K. Uncertainty estimated as 1,3-C_4H_6 uncertainty.*
C_4H_6	9,7	$\sigma = a_0 + a_1T$ $a_0 = 1.9421$ $a_1 = 0.0010984$		[46,47]	

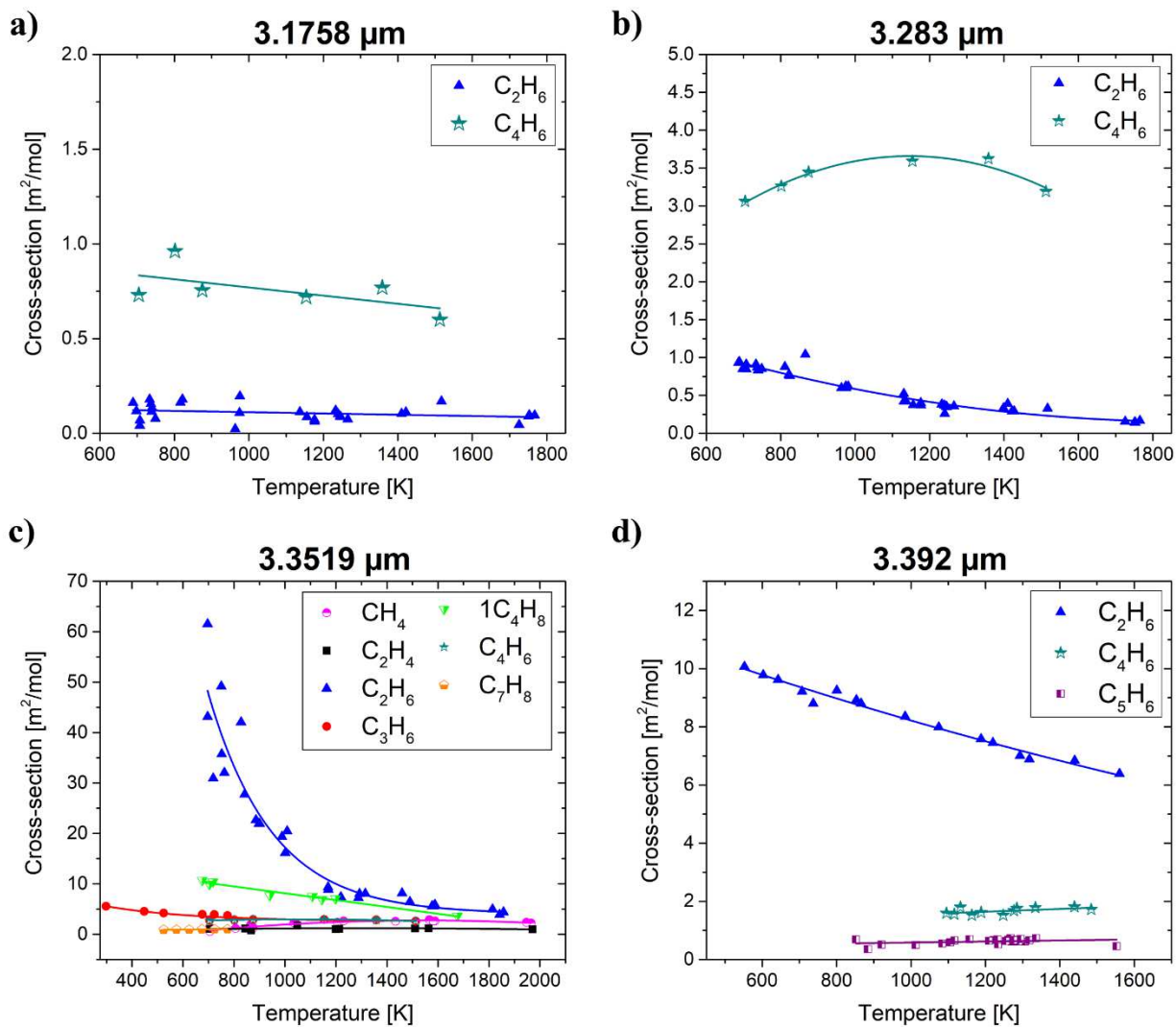| C_5H_6 | 9,8 | $\sigma = a_0 + a_1T + a_2T^2 + a_3T^3$ | $n = 22$ | New | Correlation valid between 800 K and |
		$a_0 = -73.92686$	$\nu = 18$		1600 K.
		$a_1 = 0.20195$	$RSS = 0.14132$		
		$a_2 = -1.64928E - 4$	$t_{95} = 2.101$		
		$a_3 = 4.32314E - 8$	$s_{TT} = 2.15E5$		
			$\bar{T} = 1263.73$		

508

509

510

511

512

Fig. B.1. Experimental cross-section measurements to complete the cross-section matrix. (a) Measurements at 3.1758 µm, (b) 3.283 µm, (c) 3.3519 µm, and (d) 3.392 µm.

513

514

515

516

517

518

527 **References**

528

529 [1] Hanson RK, Davidson DF. Recent advances in laser absorption and shock tube methods for

530 studies of combustion chemistry. Prog Energy Combust Sci 2014;44:103–14.

531 doi:10.1016/j.pecs.2014.05.001.

532 [2] Xu R, Wang K, Banerjee S, Shao J, Parise T, Zhu Y, et al. A physics-based approach to modeling

533 real-fuel combustion chemistry – II. Reaction kinetic models of jet and rocket fuels. Combust

534 Flame 2018;193:520–37. doi:10.1016/j.combustflame.2018.03.021.

535 [3] Wang H, Xu R, Wang K, Bowman CT, Hanson RK, Davidson DF, et al. A physics-based

536 approach to modeling real-fuel combustion chemistry - I. Evidence from experiments, and

537 thermodynamic, chemical kinetic and statistical considerations. Combust Flame 2018;193:502–

538 19. doi:10.1016/j.combustflame.2018.03.019.

539 [4] Xu R, Wang K, Banerjee S, Shao J, Parise T, Zhu Y, et al. A physics-based approach to modeling

540 real-fuel combustion chemistry – III. Reaction kinetic model of JP10. Combust Flame

541 2018;193:520–37. doi:10.1016/j.combustflame.2018.03.021.

542 [5] Wang K, Xu R, Parise T, Shao J, Movaghar A, Lee DJ, et al. A physics-based approach to

543 modeling real-fuel combustion chemistry – IV. HyChem modeling of combustion kinetics of a

544 bio-derived jet fuel and its blends with a concentional Jet A. Combust Flame 2018;198:477–89.

545   doi:10.1016/j.combustflame.2018.03.021.

546   [6]   Hanson RK, Davidson DF. Advances in shock tube techniques for fundamental studies of

547   combustion kinetics. 25th ICDERS 2015:1–5.

548   [7]   Goldenstein CS, Spearrin RM, Jeffries JB, Hanson RK. Infrared laser-absorption sensing for

549   combustion gases. Prog Energy Combust Sci 2017;60:132–76. doi:10.1016/j.pecs.2016.12.002.

550   [8]   Olson DB, Mallard WG, Gardiner WC. High Temperature Absorption of the 3.39 µm He-Ne

551   Laser Line by Small Hydrocarbons. Appl Spectrosc 1978;32:489–93.

552   doi:10.1366/000370278774330892.

553   [9]   Hidaka Y, Higashihara T, Ninomiya N, Oki T, Kawano H. Thermal isomerization and

554   decomposition of 1,2□butadiene in shock waves. Int J Chem Kinet 1995;27:331–41.

555   doi:10.1002/kin.550270404.

556   [10]   Koike T, Gardiner WC. High-Temperature Absorption of the 3.39 µm He-Ne Laser Line by

557   Acetylene, Ethylene, and Propylene. Appl Spectrosc 1980;34:81–4.

558   doi:10.1366/0003702804730899.

559   [11]   Tsuboi T, Inomata K, Tsunoda Y, Isobe A, Nagaya K. Light Absorption by Hydrocarbon

560   Molecules at 3.392 µm of He-Ne Laser. Jpn J Appl Phys 1985;24:8–13.

561   [12]   Sur R, Wang S, Sun K, Davidson DF, Jeffries JB, Hanson RK. High-sensitivity interference-free

562   diagnostic for measurement of methane in shock tubes. J Quant Spectrosc Radiat Transf

563   2015;156:80–7. doi:10.1016/j.jqsrt.2015.01.023.

564   [13]   Pyun SH, Cho J, Davidson DF, Hanson RK. Interference-free mid-IR laser absorption detection

565   of methane. Meas Sci Technol 2011;22. doi:10.1088/0957-0233/22/2/025303.

566   [14]   Pilla GL, Davidson DF, Hanson RK. Shock tube/laser absorption measurements of ethylene time-

567   histories during ethylene and n-heptane pyrolysis. Proc Combust Inst 2011;33:333–40.

568   doi:10.1016/j.proci.2010.06.146.

569   [15]   MacDonald ME, Ren W, Zhu Y, Davidson DF, Hanson RK. Fuel and Ethylene Measurements

570   during n-dodecane, methylcyclohexane, and iso-cetane pyrolysis in shock tubes. Fuel

571   2013;103:1060–8. doi:10.1016/j.fuel.2012.09.068.

572   [16]   Ren W, Davidson DF, Hanson RK. IR Laser Absorption Diagnostic for C2H4 in Shock Tube

573   Kinetics Studies. Int J Chem Kinet 2011;129. doi:10.1002/kin.20599.

574   [17]   Stranic I, Hanson RK. Laser absorption diagnostic for measuring acetylene concentrations in

575   shock tubes. J Quant Spectrosc Radiat Transf 2014;142:58–65. doi:10.1016/j.jqsrt.2014.03.024.

576   [18]   Spearrin RM, Li S, Davidson DF, Jeffries JB, Hanson RK. High-temperature iso-butene

577   absorption diagnostic for shock tube kinetics using a pulsed quantum cascade laser near 11.3 μm.

578   Proc Combust Inst 2015;35:3645–51. doi:10.1016/j.proci.2014.04.002.

579   [19]   Parise TC, Davidson DF, Hanson RK. Development of a two-wavelength IR laser absorption

580   diagnostic for propene and ethylene. Meas Sci Technol 2018;29. doi:10.1088/1361-6501/aab02b.

581   [20]   Parise T, Davidson DF, Hanson RK. Shock tube/laser absorption measurements of the pyrolysis

582   of a bimodal test fuel. Proc Combust Inst 2017;36:281–8. doi:10.1016/j.proci.2016.07.081.

583   [21]   Pinkowski N, Ding Y, Johnson SE, Wang Y, Parise T, Davidson DF, et al. A multi-wavelength

584   speciation framework for high-temperature hydrocarbon pyrolysis. J Quant Spectrosc Radiat

585   Transf 2018;225:180–205. doi:10.1016/J.JQSRT.2018.12.038.

586   [22]   Wang K, Villano SM, Dean AM. Experimental and kinetic modeling study of butene isomer

587   pyrolysis: Part II. Isobutene. Combust Flame 2017;176:23–37.

588   doi:10.1016/j.combustflame.2016.07.036.

589   [23]   Grant M, Boyd S. CVX: Matlab software for disciplined convex programming, version 2.0 beta.

590   http://cvxr.com/cvx n.d.

591   [24]   Grant M, Boyd SP. Graph implementations for nonsmooth convex programs, Recent Advances in

592   Learning and Control (a tribute to M. Vidyasagar), V. Blondel, S. Boyd, and H. Kimura, editors,

593   pages 95-110. Springer; 2008. doi:10.1109/ISIC.2014.6967596.

594   [25]   Campbell MF, Haylett DR, Davidson DF, Hanson RK. AEROFROSH: a shock condition

595   calculator for multi-component fuel aerosol-laden flows. Shock Waves 2016;26:429–47.

596   doi:10.1007/s00193-015-0582-3.

597   [26]   Gauthier BM, Davidson DF, Hanson RK. Shock tube determination of ignition delay times in

598   full-blend and surrogate fuel mixtures. Combust Flame 2004;139:300–11.

599   doi:10.1016/j.combustflame.2004.08.015.

600   [27]   Alrefae M, Es-Sebbar ET, Farooq A. Absorption cross-section measurements of methane, ethane,

601   ethylene and methanol at high temperatures. J Mol Spectrosc 2014;303:8–14.

602   doi:10.1016/j.jms.2014.06.007.

603   [28]   Wang S, Parise T, Johnson SE, Davidson DF, Hanson RK. A new diagnostic for hydrocarbon

604   fuels using 3.41-µm diode laser absorption. Combust Flame 2017;186:129–39.

605   doi:10.1016/j.combustflame.2017.07.026.

606   [29]   Al Shoaibi A, Dean AM. Kinetic analysis of C4 alkane and alkene pyrolysis: Implications for

607   SOFC operation. J Fuel Cell Sci Technol 2010;7:0410151–8. doi:10.1115/1.4000677.

608   [30]   Zhang Y, Cai J, Zhao L, Yang J, Jin H, Cheng Z, et al. An experimental and kinetic modeling

609   study of three butene isomers pyrolysis at low pressure. Combust Flame 2012;159:905–17.

610   [31]   Pan L, Hu E, Zhang J, Tian Z, Li X, Huang Z. A high pressure shock tube study of 1-butene

611   oxidation and its comparison with n-butane and alkenes. Fuel 2015;157:21–7.

612   doi:10.1016/j.fuel.2015.04.062.

613   [32]   Schenk M, Leon L, Moshammer K, Oßwald P, Zeuch T, Seidel L, et al. Detailed mass

614   spectrometric and modeling study of isomeric butene flames. Combust Flame 2013;160:487–503.

615   doi:10.1016/j.combustflame.2012.10.023.

616   [33]   Manion JA, Awan IA. Evaluated kinetics of terminal and non-terminal addition of hydrogen

617   atoms to 1-alkenes: A shock tube study of H + 1-butene. J Phys Chem A 2015;119:429–41.

618   doi:10.1021/jp5110856.

619   [34]   Trenwith AB. 1 -Butene, 3-Methyl-l-Butene, and of 3:3-Dimethyl-l -Butene and the Resonance

620   Energy of the Allyl, Methyl Allyl and Dimethyl Allyl Radicals 1970:2805–11.

621   [35]   Bryce BYWA, Kebarle P. The thermal decomposition of 1-butene and 1-butene-4-d3 1958.

622   [36]   Corcoran WH. Pyrolysis of 1-Butene and Cis -2 -Butene 1976.

623 [37] Es-Sebbar E, Jolly A, Benilan Y, Farooq A. Quantitative mid-infrared spectra of allene and

624   propyne from room to high temperatures. J Mol Spectrosc 2014;305:10–6.

625   doi:10.1016/j.jms.2014.09.004.

626 [38] Stranic I, Pyun SH, Davidson DF, Hanson RK. Multi-species measurements in 1-butanol

627   pyrolysis behind reflected shock waves. Combust Flame 2012;159:3242–50.

628   doi:10.1016/j.combustflame.2012.06.005.

629 [39] Stranic I, Pang GA, Hanson RK, Golden DM, Bowman CT. Shock tube measurements of the rate

630   constant for the reaction ethanol + OH. J Phys Chem A 2014;118:822–8. doi:10.1021/jp410853f.

631 [40] Zhou CW, Li Y, Burke U, Banyon C, Somers KP, Ding S, et al. An experimental and chemical

632   kinetic modeling study of 1,3-butadiene combustion: Ignition delay time and laminar flame speed

633   measurements. Combust Flame 2018;197:423–38. doi:10.1016/j.combustflame.2018.08.006.

634 [41] Sharpe SW, Johnson TJ, Sams RL, Chu PM, Rhoderick GC, Johnson PA. Gas-Phase Databases

635   for Quantitative Infrared Spectroscopy. Appl Spectrosc 2004;58:1452–61.

636 [42] Lattanzi F, Di Lauro C, Vander Auwera J. Toward the understanding of the high resolution

637   infrared spectrum of C2H6 near 3.3 μm. J Mol Spectrosc 2011;267:71–9.

638   doi:10.1016/j.jms.2011.02.003.

639 [43] Es-Sebbar ET, Benilan Y, Farooq A. Temperature-dependent absorption cross-section

640   measurements of 1-butene (1-C4H8) in VUV and IR. J Quant Spectrosc Radiat Transf

641   2013;115:1–12. doi:10.1016/j.jqsrt.2012.09.014.

642 [44] Klingbeil AE, Jeffries JB, Hanson RK. Temperature-dependent mid-IR absorption spectra of

643   gaseous hydrocarbons. J Quant Spectrosc Radiat Transf 2007;107:407–20.

644   doi:10.1016/j.jqsrt.2007.03.004.

645 [45] Gordon IE, Rothman LS, Hill C, Kochanov R V., Tan Y, Bernath PF, et al. The HITRAN 2016

646   molecular spectroscopic database. J Quant Spectrosc Radiat Transf 2017;203:3–69.

647   doi:10.1016/j.jqsrt.2017.06.038.

648 [46] Strand CL, Ding Y, Johnson SE, Hanson RK. Measurement of the mid-infrared absorption

649　　　spectra of ethylene (C2H4) and other molecules at high temperatures and pressures. J Quant

650　　　Spectrosc Radiat Transf 2018;222–223:122–9. doi:10.1016/j.jqsrt.2018.10.030.

651　[47]　Johnson SE, Davidson DF, Hanson RK. Shock tube/laser absorption measurements of the

652　　　pyrolysis of JP-10 fuel. AIAA SciTech Forum 2019:1–7. doi:10.2514/6.2019-0575.

653　[48]　Chrystie RSM, Nasir EF, Farooq A. Propene concentration sensing for combustion gases using

654　　　quantum-cascade laser absorption near 11 μm. Appl Phys B Lasers Opt 2015;120:317–27.

655　　　doi:10.1007/s00340-015-6139-4.

656

Technical Report Documentation Page

1. Report No.	2. Government Accession No.	3. Recipient's Catalog No.
4. Title and Subtitle		5. Report Date
		6. Performing Organization Code
7. Author(s)		8. Performing Organization Report No.
9. Performing Organization Name and Address		10. Work Unit No. (TRAIS)
		11. Contract or Grant No.
12. Sponsoring Agency Name and Address		13. Type of Report and Period Covered
		14. Sponsoring Agency Code
15. Supplementary Notes		
16. Abstract		
17. Key Words	18. Distribution Statement	

19. Security Classif. (of this report) Unclassified	20. Security Classif. (of this page) Unclassified	21. No. of Pages	22. Price

Form DOT F 1700.7 (8-72)   Reproduction of completed page authorized